IPSJ Transactions on Computer Vision and Applications Vol. 3 172–185 (Dec. 2011)

Research Paper

Robust Estimation of Light Directions and Albedo Map of an Object of Known Shape

Takehiro Tachikawa,[†1] Shinsaku Hiura[†2] and Kosuke Sato[†1]

This paper describes a method to determine the direction of a light source and the distribution of diffuse reflectance from two images under different lighting conditions. While most inverse-rendering methods require 3 or more images, we investigate the use of only two images. Using the relationships between albedo and light direction at 6 or more points, we firstly show that it is possible to simultaneously estimate both of these if the shape of the target object is given. Then we extend our method to handle a specular object and shadow effect by applying a robust estimation method. Thorough experimentation shows that our method is feasible and stable not only for well controlled indoor scenes, but also for an outdoor environment illuminated by sunlight.

1. Introduction

In this paper, we propose a method to simultaneously estimate both the direction of the light source and the diffuse reflectance from two images of an object with known shape under different lighting conditions.

In recent years, 3-D representations of existing objects instead of photographs have become popular in various fields such as recording, presentation, and communication. Since the shape of an object is essential in a 3-D representation, shape measurement methods have been intensively studied to realize precise, robust and fast acquisition. Currently, a variety of shape measurement equipment such as laser rangefinders is commercially available, and we can measure the shape of most objects with sufficient precision using these. On the other hand, the distribution of the reflectance property on the object surface is not easy to measure precisely nor has it been commercialized. In other words, measurement of a photometric property has been less explored than that of geometric parameters.

As the representation of the photometric surface property, texture mapping using simply taken pictures is often used. However, such a shortcut detracts from the merits of 3-D representations because the observed intensity of a fixed point on the object is not constant for various lighting conditions. To reproduce the correct intensity change according to the environmental parameters, the optical phenomena of reflection should be simulated using both surface and lighting properties. Therefore, the lighting condition and surface reflectance should be separated from the taken picture, which is a product of the interaction between light and the object.

2. Related Work

Photometric analysis of images has been intensively explored in the field of computer vision. Since the intensity of an object is determined by the rendering equation [1] which integrates the lighting distribution, reflectance property (BRDF), and surface normal, we can partially estimate these using other known parameters using the input images.

Shape reconstruction by analyzing the intensity change according to the lighting condition is a major topic known as shape from shading [2] or photometric stereo [3),4)]. However, as described before, estimation of a surface property is not as easy as measurement of the shape of the object. Therefore, estimation of a photometric property such as the lighting condition or reflectance is also worth exploring.

2.1 Recovery of Illumination Using Specular

If there is a sphere with polished metal surface in a scene, we can directly recover the lighting condition of the scene as Light Probe method by Debevec [5)]. Correspondingly, most studies for estimating lighting conditions exploits specular reflection. Since the geometric relationships among the light, mirror and camera is trivial, main topic of those papers are simultaneous estimation of illumination map and reflectance property of surface such as parametric or nonparametric BRDF models. Ikeuchi proposed a method to estimate the parameters of the

†1 Graduate School of Engineering Science, Osaka University
†2 Graduate School of Information Sciences, Hiroshima City University

Torrance-Sparrow reflection model and direction to the light source from a pair of range and intensity images [6]. Romeiro et al. [7] much extend the way of analysis to simultaneously estimate BRDF and lighting condition using the framework of blind deconvolution in signal processing area. However, this method assumes that the reflectance is uniform over the whole object. Ramamoorthi et al. [8] try to extend their method for textured object by incorporating priors, but they also pointed out that the factorization of lighting and texture is ambiguous. Zickler et al. [9] also assume that the distribution of BRDF is smooth. Therefore, methods to separate diffuse and specular reflection components by using color or polarization are also explored. Sato proposed a method to recover the distribution of reflectance parameters on the object [10]. At first, specular reflection is separated from diffuse reflection, then the parameters are estimated for each region segmented by the hue of the object. This method assumes that the color of the body reflection is different from that of the light source. Hara et al. [11),12] also estimate the illumination condition using specular components.

2.2 Estimating Illumination Conditions Using Diffuse Components

Though the specular reflection is useful to estimate the illumination conditions, it is not applicable for diffuse object. Most natural objects or historic constructions are diffuse, and curved shiny object is rarely observed in outdoor scene. Unfortunately, Lambertian surface does not give us enough information to estimate the illumination maps [13] because the broad collection of incident light limits the bandwidth of spatial frequency of lighting condition. Especially, as described in Section 5.3, multiple light sources can be substituted by a single light at average direction when the shadowing effect is not observed. Therefore, the estimation of light direction is more reasonable than recovering illumination maps when we only use Lambertian reflection components. It is trivial that simultaneous estimation of reflectance map and light direction using a single image is impossible. If multiple images can be used, estimation of a dense reflectance map is possible. The photometric stereo [3] method gives the albedo of an object for each pixel from three images with known light sources. This method has been extended to the case of unknown light sources, but there is an ambiguity between the shape of the object and direction to the light source, which is called the Bas-Relief ambiguity [14], and additional information such as shadow, specular or object shape is necessary to stabilize the solution.

2.3 Contributions

Most methods based on photometric stereo require 3 or more images under different lighting conditions [15], and this limits the variety of applications. Therefore, in this paper, we will discuss the minimum number of input images to estimate the albedo map if we already know the shape of the object. If it were possible to recover both reflectance and lighting direction from a single image, this would be very useful. However, in theory this is impossible because identical images could be observed with different lighting conditions and coordinated textures. Then, what about 2 input images? Surprisingly, the case of 2 images has not been well investigated, whereas cases of a single image or 3 images have been extensively researched. This paper provides an answer to this question. In this paper, we prove that both the lighting directions and albedo map of an object of known shape can be recovered from 2 images taken under different lighting conditions. As shown by the results, our theory is not only new but also practical for real images when it is combined with a robust estimation technique. Although our method initially assumes Lambert reflection, the robust estimation makes it applicable to specular reflection, shadowing and multiple light sources. Moreover, we conducted an experiment using the movement of sunlight to emphasize the advantage of our method. Methods based on a photometric stereo framework are not applicable to the movement of sunlight because the sun moves in a circle.

Simultaneous estimation of light directions and albedo maps is not only useful by itself but also very helpful if combined with specular analysis methods described in Section 2.1. As described before, the separation of diffuse and specular components as preprocessing improves the performance of recovery of illumination maps. This paper also contribute to give an analytic and well-conditioned solution of recovering albedo map under unknown lighting directions, and it will augment the validity of various methods based on statistics, example-base or signal-processing.

2.4 Limitations

Our method stands on the direct observation of diffuse reflection components in the images. Using robust estimation algorithms, our method successfully exclude outliers which affected by shadow, specular or interreflection. However, if most

visible part of the object is covered by such nonlinear effects, our algorithm will fail. One typical case of such failure case is observing shiny curved object in global illumination conditions, because most pixel is affected by specular component. Fortunately, such case is well covered by the methods described in Section 2.1. Contrary, our method is suitable for the object with textured surface under locally distributed light sources.

3. Simultaneous Estimation of Light Direction and Diffuse Reflectance

Figure 1 gives an outline of the proposed method. Our method assumes that we have two images, under different lighting conditions, of an object whose shape is known. First we derive a constraint between the two intensity values and the surface normal at each point in the following section.

3.1 Constraint between Two Images

In this section, we derive an equation giving a constraint between two images of an object and its shape. To simplify the discussion, we assume the following conditions, although some of these are relaxed later.

- Point correspondences between the two images are given.
- The normal at each point on the image is known.
- Illumination is from a single, uniform, parallel light, the intensity and direction of which are unknown.
- Surface reflectance of the object is Lambertian, neither known nor uniform.

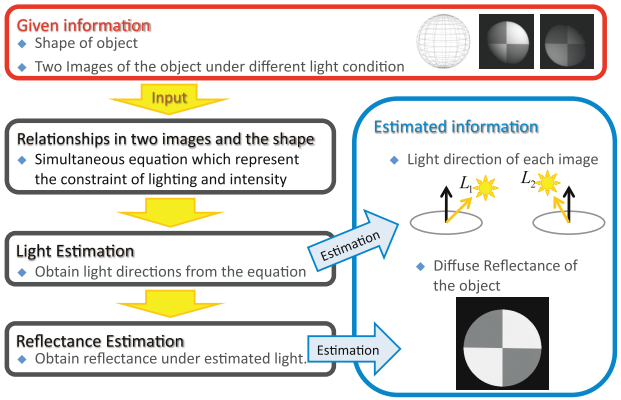

Fig. 1 Outline of proposed method.

The intensity at a point I_p $(1 \leq p \leq n)$ is denoted by Lambert's reflection model as

$$I_p = \rho_p N_p \cdot L \tag{1}$$

where N_p denotes the normal vector at point p, L denotes the light direction, and ρ_p denotes Lambertian reflectance. Since we have two images with point correspondences, we have the following two equations with a common normal vector and reflectance

$$I_{1p} = \rho_p N_p \cdot L_1 \tag{2}$$

$$I_{2p} = \rho_p N_p \cdot L_2 \tag{3}$$

where I_{kp} and L_k are the intensity and light direction, respectively, of the k-th image $(k = 0, 1)$. Element values of vectors

$$L_1 = [L_{1x}\ L_{1y}\ L_{1z}]^T$$
$$L_2 = [L_{2x}\ L_{2y}\ L_{2z}]^T$$
$$N_p = [N_{px}\ N_{py}\ N_{pz}]^T$$

are used to expand the two equations (2) and (3), and we have

$$I_{1p} = \rho_p(N_{px}L_{1x} + N_{py}L_{1y} + N_{pz}L_{1z}) \tag{4}$$

$$I_{2p} = \rho_p(N_{px}L_{2x} + N_{py}L_{2y} + N_{pz}L_{2z}). \tag{5}$$

In the equations above, the reflectance parameter ρ_p is the common value. Therefore, it is eliminated to derive the single equation

$$I_{2p}N_{px}L_{1x} + I_{2p}N_{py}L_{1y} + I_{2p}N_{pz}L_{1z} - I_{1p}N_{px}L_{2x} - I_{1p}N_{py}L_{2y} - I_{1p}N_{pz}L_{2z} = 0 \tag{6}$$

with its vector representation

$$m_p^T L' = 0 \tag{7}$$

where

$$L' = \begin{bmatrix} L_{1x} \\ L_{1y} \\ L_{1z} \\ L_{2x} \\ L_{2y} \\ L_{2z} \end{bmatrix}, m_p = \begin{bmatrix} I_{2p}N_{px} \\ I_{2p}N_{py} \\ I_{2p}N_{pz} \\ -I_{1p}N_{px} \\ -I_{1p}N_{py} \\ -I_{1p}N_{pz} \end{bmatrix}.$$

As assumed before, the direction of the incoming light is uniform over all the pixels in a single image. In other words, the vector of the lighting condition L' is common to all pixels, while m_p (information about pixel intensity and normal) is independent for each pixel. Therefore, we can combine all the pixels in the matrix representation

$$ML' = 0 \tag{8}$$

where $M = [m_1 \cdots m_n]$. In the next section, we show how to obtain L', which contains both light directions, L_1 and L_2.

3.2 Rank of matrix M

If matrix M has full rank ($rank(M) = 6$), the solution must be $L' = 0$. However, L' should be a nontrivial solution because we assume a non-zero light source ($L_1 \neq 0$, $L_2 \neq 0$) to derive Eq. (8). Therefore, the rank of matrix M is less than 6.

If the rank of matrix M is 5, L' is uniquely determined with scale ambiguity. In the case of singular conditions, for example, all normal vectors are coplanar or the directions of the two light sources are identical, the rank of matrix M is less than 5. Except in such singular cases, we confirm that the rank of matrix M reaches 5 by simulation in Section 7.

3.3 Estimation of Lighting Condition

The nontrivial solution of L' in Eq. (8) is equivalent to the orthogonal complement of matrix M. If the rank of M is equal to 5, the orthogonal complement is 1-D space and we can estimate the directions to the two light sources and their intensity ratio. The orthogonal complement can be calculated by principal component analysis (PCA) of matrix M.

In principle, the absolute intensity of a light source cannot be estimated, because an object with half the reflectance under a light source that is twice as bright gives exactly the same image. In other words, the intensity of the light source and reflectance have scalar indefiniteness. However, the intensity ratio of two light sources L_1, L_2 can be estimated.

4. Robust Estimation of Nonlinear Photometric Phenomena

In this section, we introduce a method for dealing with nonlinear photometric phenomena, caused by specular reflection or shadow, by applying robust estimation. As an extension of photometric stereo, a method to avoid the interference of highlights and shadows have been proposed [16], but it requires an additional input image under different lighting condition. In contrast, the method we describe below does not require additional images.

4.1 Random Sample Consensus

In Section 3.1, we derived the equation assuming Lambertian reflection. However, actual scenes usually have specular reflection, interreflection, and shadows. Such optical phenomena act as nonlinear relationships between the lighting conditions and luminance of the scene. To deal with such effects, we use a robust estimation method called Random Sample Consensus (RANSAC) [17] to find the value of L'.

In general, the nonlinear phenomena described above are observed locally. The regions of specular reflection and shadow are limited by the shape of the object and light direction, while interreflection is observed at concave regions. Therefore, pixels affected by such effects could be treated as outliers, and RANSAC effectively eliminates them.

The procedure for robust estimation is as follows.

(1) Randomly select R pixels from $m_1, \cdots, m_n$.
(2) As described in Section 3.3, calculate the value of L' using matrix M consisting of the selected R pixels only.
(3) For all pixels $m_1, \cdots, m_n$, calculate the reprojection error $\left|m_p^T L' - 0\right|$ using the estimated L'.
(4) Count the number of pixels whose error is within the threshold T.
(5) Repeat steps (1)–(4), and take the value of L' when the number of pixels within the threshold is the largest.

Equation (8) indicates that the number of samples R should be equal to or greater

than 6. The threshold T should be set to allow for variance caused by camera noise. In the experiments, we use $0.02 \leq T \leq 0.04$ if the maximum value of pixel intensity is 1.

4.2 Estimation of Albedo

By using the estimated direction of the light sources, we can estimate the distribution of albedo. By solving Eqs. (4) and (5), we get

$$\rho_{1p} = \frac{I_{1p}}{(N_{px}L_{1x} + N_{py}L_{1y} + N_{pz}L_{1z})} \tag{9}$$

$$\rho_{2p} = \frac{I_{2p}}{(N_{px}L_{2x} + N_{py}L_{2y} + N_{pz}L_{2z})} \tag{10}$$

and we can estimate the albedo of all points using either image 1 or 2.

Since actual data includes noise, the values from Eqs. (9) and (10) for a corresponding point could be different. In particular, if the angle between the normal of the surface and the light direction is large, the values of both the denominator and numerator will be small and the calculation becomes unstable. Therefore, if both values from the two images are valid, we use the weighted average of Eqs. (9) and (10),

$$\rho_p = \frac{\omega_1}{\omega_1 + \omega_2}\frac{I_{1p}}{\omega_1} + \frac{\omega_2}{\omega_1 + \omega_2}\frac{I_{2p}}{\omega_2} = \frac{I_{1p} + I_{2p}}{\omega_1 + \omega_2} \tag{11}$$

where ω_1 and ω_2 are the values of the denominators in Eqs. (9) and (10), respectively.

4.3 Exclusion of a Pixel with Non-linear Effects

If the pixel used to estimate the albedo is affected by specular reflection or shadow, the reconstructed value of reflectance will be incorrect. Therefore, any pixel with such an effect should be discriminated and the value of either Eq. (9) or (10) without nonlinear effects is used.

The occurrence of attached shadow can be determined by the angle between the light direction and the surface normal. If the inner product of light vector L and normal N is negative ($L \cdot N_p < 0$), the pixel under lighting condition L is not used, and the albedo estimated from the other image is used. Since we have geometric information of the object, we can also determine if the observed point is in the cast shadow or not.

The position of specular reflection in the image can also be calculated using the surface normal. However, in practice, the given surface normal is not always sufficiently accurate to estimate precisely the specular reflection. Therefore, we also use the values of the estimated albedos, ρ_{1p} and ρ_{2p}. If the difference between the two estimated albedos exceeds a predetermined threshold, we simply select the lower value instead of merging the two albedos by Eq. (11).

5. Discussion on the Lighting Conditions

As described above, the conditions on the surface property have been relaxed to a shiny surface although we started with the assumption of Lambert reflection. We have also explained a method to handle the attached and cast shadow using the RANSAC algorithm followed by determination of the shadow region. In this section, we discuss the lighting conditions that can be handled by our method.

5.1 Condition for the Area of Inliers

Since we use a RANSAC algorithm to exclude outliers, the number of inliers should be larger than any other false consistent model. Inliers can be defined as non-specular pixels lit from both light sources, while the area lit from a unilateral light source could be regarded as a false model.

If the number of inliers exceeds half the number of pixels, the condition for RANSAC is always satisfied. In this case, the estimation will always be successful if the number of RANSAC trials is sufficiently large. Furthermore, a scene could have multiple false models in the image. As shown in **Fig. 2**, a solution from an area that is not lit from light source 1 (R_1) is not usually consistent with the other area (R_2). Therefore, the condition for successful RANSAC estimation is

$$R_{12} > max(R_1, R_2). \tag{12}$$

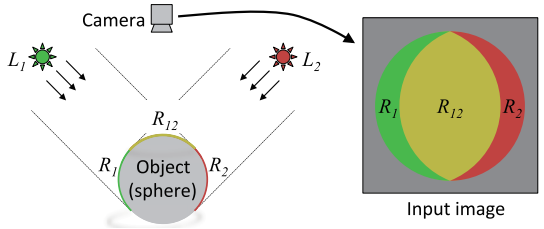

Fig. 2 Three regions on a sphere. R_{12} is an inlier illuminated from both light sources, while R_1 and R_2 are regions of unilateral attached shadow.

It is trivial to prove $R_{12} + R_1 + R_2 = 1$, and therefore, the necessary condition for successful RANSAC calculation is $R_{12} > 1/3$.

5.2 Number of RANSAC Trials

For successful RANSAC calculation, we must have more than one successful trial that extracts all the samples from an inlier region. Since the number of samples used to solve Eq. (8) is 6, we can calculate the possibility of a successful case by the sixth power of the proportion of the inlier region R_{12}. Therefore, the expected value for successful sampling by t trials can be expressed as

$$E = t \times (R_{12})^6. \tag{13}$$

Therefore, the worst case of inlier region (Section 5.1) needs $t = 729$ trials to have more than 1 expectation because $(R_{12})^6 = (1/3)^6 = 1/729$.

The possibility of successful RANSAC calculation by t trials is

$$Q_{12} = 1 - (1 - (R_{12})^6)^t. \tag{14}$$

For example, the possibility of successful estimation under the worst condition $R_{12} = 1/3$ with $t = 729$ trials is 63.2%. In our experiment, we used $t = 1000$ trials. In this case, the expected value is $E = 1.37$ and the possibility of successful estimation is $Q_{12} = 0.75$ under the worst condition $R_{12} = 1/3$. However, the possibility improves significantly if we have slightly more inliers, for example, $Q_{12} = 0.9999998$ if $R_{12} = 1/2$.

5.3 Case of Simultaneous Multiple Light Sources

Our method assumes a single distant light source for each observed image. However, we can estimate the average direction of multiple light sources because we use a Lambert reflection model for the estimation.

Let us assume a region lit by s light sources. If a pixel is not in the shadow region of any light source, Eq. (1) can be rewritten as

$$I_p = \sum_{i=0}^{s} \rho_p N_p \cdot L_i = \rho_p N_p \cdot \sum_{i=0}^{s} L_i. \tag{15}$$

Therefore, the multiple point light sources $L_1 \cdots L_s$ can be considered a single light source $L = \sum_{i=0}^{s} L_i$, and the proposed method is still valid in the case of multiple light sources. However, this assumption is valid only in a region that is lit from all the light sources. Furthermore, an individual light direction cannot be estimated. We show the experimental results for this case in a later section.

6. Simulation Experiments

In this section, we give an evaluation of our theory including a discussion on the rank of matrix M. While the shape of the object is based on the actual object measured by a rangefinder, images are rendered computationally with given light directions and reflectance.

Prior to rendering, the shape of the object shown in Fig. 8 (a) is measured using a rangefinder (Minolta VIVID 910). The measured shape of the object is shown in Fig. 8 (b). While significant error is observed around the edge of the reflectance change, it does not affect the result of the simulation because the image is rendered with the measured shape.

The reflectance map attached to the object is shown in **Fig. 3** (a). We rendered the images in two ways, with and without specular reflection. To highlight the effect of robust estimation, we give the results using all the sample points and the RANSAC method for comparison.

6.1 Case without Specular Reflection

To distinguish the estimated values from the ground truth, the estimated light directions are denoted as $\hat{L_1}$ and $\hat{L_2}$. Evaluation of the estimated light directions is given in **Table 1**, while the contribution rate of the PCA calculation is shown in **Table 2**. Since no nonlinear effect is included, the directions of the light sources are estimated correctly without errors. The rank of matrix M is 5 because the 6th eigenvalue of PCA is zero, whereas the 5th is nonzero.

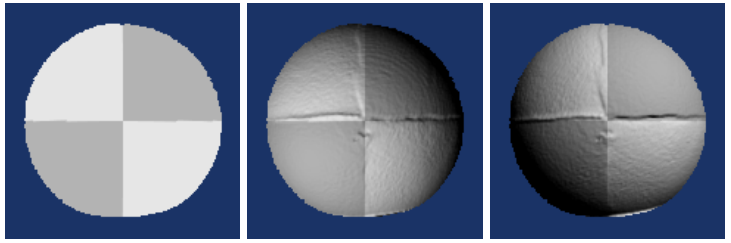

(a) (b) (c)

Fig. 3 Albedo map and rendered images used in the simulation without specular reflection. (a) Albedo map used to render images for simulation, (b) illuminated by L_1, (c) illuminated by L_2.

Table 1 Error in estimated light source direction in simulation experiment.

	Error in L_1 ($\|\hat{L_1} - L_1\|$)	Error in L_2 ($\|\hat{L_2} - L_2\|$)
without specular (estimated from all samples)	0.000000	0.000000
without specular (robust estimation)	0.000000	0.000001
with specular (estimated from all samples)	0.033353	0.022228
with specular (robust estimation)	0.003822	0.002221

Table 2 Contribution rate of PCA in simulation experiments.

	1st eigenvalue	5th eigenvalue	6th eigenvalue
without specular (estimated from all samples)	0.382252	0.024376	0.000000
without specular (robust estimation)	0.485959	0.028724	0.000000
with specular (estimated from all samples)	0.374664	0.025766	0.001929
with specular (robust estimation)	0.426680	0.018154	0.000006

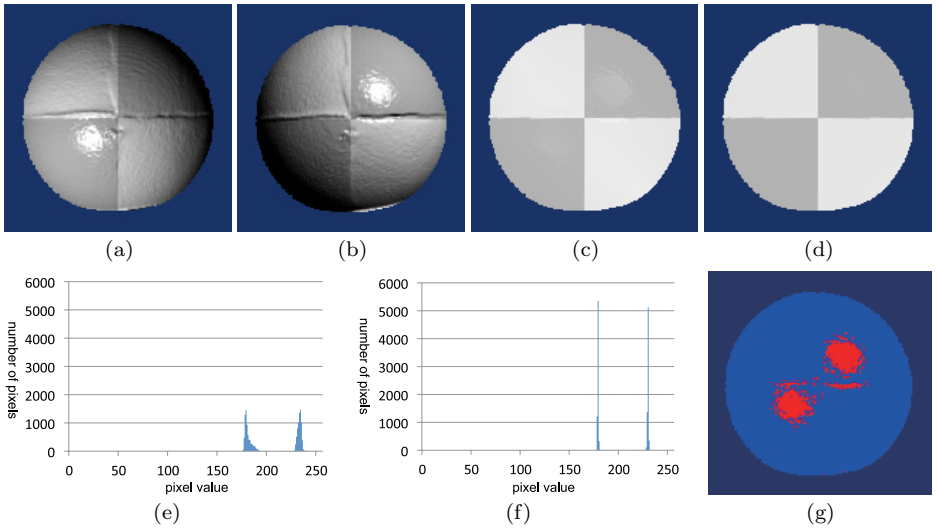

Fig. 4 Simulation with specular reflection. (a) Image illuminated by L_1, (b) image illuminated by L_2, (c) albedo map estimated using all the samples, (d) albedo map estimated using RANSAC algorithm, (e) histogram of (c), (f) histogram of (d), (g) map of outliers found by robust estimation.

6.2 Case with Specular Reflection

To render the images with specular reflection, we used Phong's reflection model given as

$$I_p = \rho_p(N_p \cdot L) + s_p(R_p \cdot V)^\alpha \quad (16)$$

where s_p denotes specular reflectance, α denotes shininess, R_p is the vector of mirror reflection, and V is the vector to the observer. Rendered images are shown in **Fig. 4** (a) and (b).

The Albedo maps estimated using all the samples and the robust algorithm are shown in Figs. 4 (c) and (d), respectively (see pdf file directly instead of printed matter). While some variation in reflectance can be seen in Fig. 4 (c), robust estimation gives uniform reflectance. Histograms of these images are shown in Figs. 4 (e) and (f). Since we use two values of reflectance on the object, the two sharp peaks in Fig. 4 (f) show that the robust method recovers the reflectance exactly.

Errors in the estimated light directions are given in Table 1, while the eigenvalues of the PCA calculation are given in Table 2. It is clear that the estimated direction of the light source using the RANSAC algorithm is better than that using all the samples, and that the last eigenvalue is also sufficiently small. Fig. 4 (g) shows the distribution of the outliers. The region of specular reflection is correctly excluded.

6.3 Experiment Investigating the Proportion of the Inlier Region

In this section we give experimental results to show the robustness of estimation against the small inlier region. The light source L_1 for image 1 and the other light source L_2 for image 2 are arranged at the left and right with angles $\pm\frac{1}{6}\pi$, $\pm\frac{1}{4}\pi$, $\pm\frac{1}{3}\pi$ [rad] for rendering images. The intensity of lights L_1 and L_2 are $L_1 = 0.5$ and $L_2 = 1.0$, respectively. Again, we applied two algorithms, with and without RANSAC.

The error in the estimated direction to the light sources is given in **Table 3**. The estimated intensity ratio of the two light sources is also shown in the

Table 3 Error in estimation of light direction and intensity.

light direction [rad] and method used	error in direction to light source 1 [rad]	error in direction to light source 2 [rad]	error in intensity ratio of two light sources
$\pm\frac{1}{6}\pi$ with all samples	0.083	0.015	0.060
$\pm\frac{1}{4}\pi$ with all samples	0.262	0.137	0.394
$\pm\frac{1}{3}\pi$ with all samples	0.491	0.391	1.732
$\pm\frac{1}{6}\pi$ by RANSAC	0.015	0.032	0.029
$\pm\frac{1}{4}\pi$ by RANSAC	0.030	0.023	0.021
$\pm\frac{1}{3}\pi$ by RANSAC	1.067	0.683	4.024×10^{14}

rightmost column of the table. The estimated albedo map is shown in **Fig. 5**. The rightmost column in Fig. 5 is the map of inliers and outliers estimated by RANSAC.

As shown in Table 3, it is evident that the estimation using all samples causes too many errors. On the contrary, the results with RANSAC are successful if the angle between the two light sources is sufficiently small. This is also confirmed by the estimated albedo map shown in Fig. 5, because the albedo and outliers are correctly estimated if the angle of the light sources is $\pm\frac{1}{6}\pi$ or $\pm\frac{1}{4}\pi$. However, in the case of $\pm\frac{1}{3}\pi$, the estimation fails. In this case, the necessary condition for the area of inliers (Section 5.1) is no longer satisfied. Overall, the experimental results show that the proposed method correctly excludes outliers caused by shadows and specular reflection if the necessary condition is satisfied.

6.4 Experiments with Simultaneous Multiple Light Sources

In this section, we give the experimental results for simultaneous multiple sources of lighting for the object. As described in Section 5.3, we can estimate the albedo map of an object by assuming the sum of multiple light sources. However, multiple light sources decrease the area of inliers because we have additional attached shadow regions on the object as shown in **Fig. 6**. Therefore, we show the results for a variety of light directions.

The intensities of all light sources are fixed at 0.5. The angle θ_1 gives the horizontal movement of the light sources. Light source L_{11} for image 1 and the other light source L_{21} for image 2 are moved to the right and left, respectively, with angles $\theta_1 = \frac{1}{12}\pi$, $\frac{1}{6}\pi$, $\frac{1}{4}\pi$, and $\frac{1}{3}\pi$ [rad]. The other angle depicting the

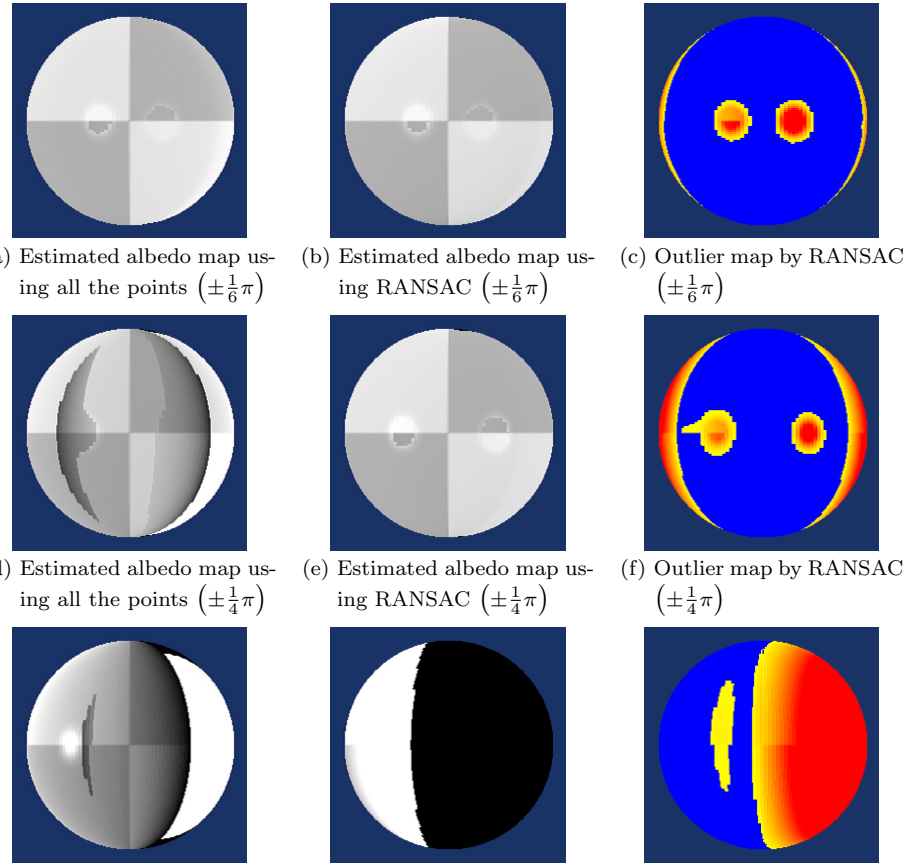

(a) Estimated albedo map using all the points $\left(\pm\frac{1}{6}\pi\right)$ (b) Estimated albedo map using RANSAC $\left(\pm\frac{1}{6}\pi\right)$ (c) Outlier map by RANSAC $\left(\pm\frac{1}{6}\pi\right)$

(d) Estimated albedo map using all the points $\left(\pm\frac{1}{4}\pi\right)$ (e) Estimated albedo map using RANSAC $\left(\pm\frac{1}{4}\pi\right)$ (f) Outlier map by RANSAC $\left(\pm\frac{1}{4}\pi\right)$

(g) Estimated albedo map using all the points $\left(\pm\frac{1}{3}\pi\right)$ (h) Estimated albedo map using RANSAC $\left(\pm\frac{1}{3}\pi\right)$ (i) Outlier map by RANSAC $\left(\pm\frac{1}{3}\pi\right)$

Fig. 5 Experimental results with respect to the proportion of inliers.

vertical movement of the light sources is θ_2. Light source L_{12} for image 1 and the other light source L_{22} for image 2 are moved up and down, respectively, with angles $\theta_2 = 0$, $\frac{1}{12}\pi$, $\frac{1}{6}\pi$, $\frac{1}{4}\pi$, and $\frac{1}{3}\pi$ [rad]. Therefore, we have 20 combinations of angles θ_1 and θ_2. Eight images in four cases with $\theta_1 = \theta_2$ are shown in **Fig. 7**.

Tables 4 and **5** show the error of estimated angles of average direction to the

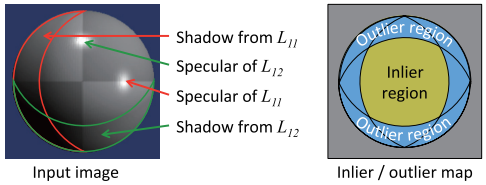

Fig. 6 Areas of inliers and outliers under two light sources for each image.

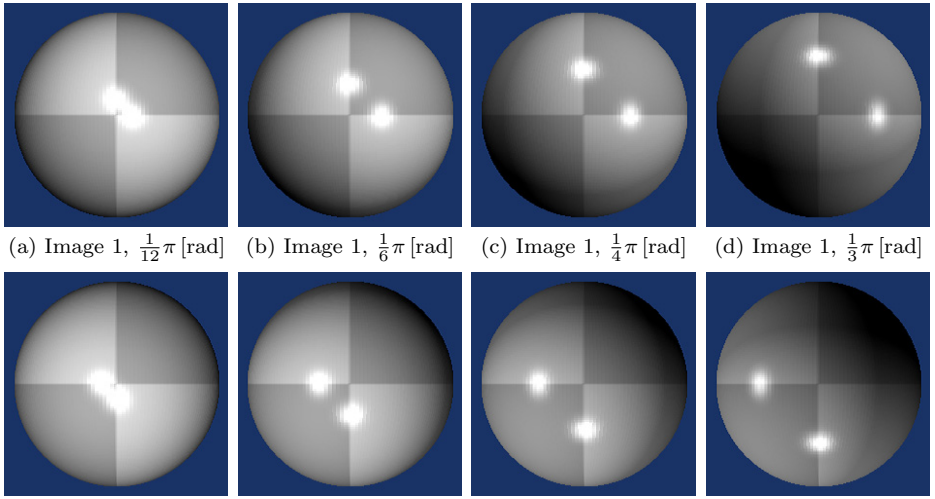

(a) Image 1, $\frac{1}{12}\pi$ [rad] (b) Image 1, $\frac{1}{6}\pi$ [rad] (c) Image 1, $\frac{1}{4}\pi$ [rad] (d) Image 1, $\frac{1}{3}\pi$ [rad]

(e) Image 2, $\frac{1}{12}\pi$ [rad] (f) Image 2, $-\frac{1}{6}\pi$ [rad] (g) Image 2, $-\frac{1}{4}\pi$ [rad] (h) Image 2, $-\frac{1}{3}\pi$ [rad]

Fig. 7 Images lit by two light sources simultaneously.

light sources. The error of estimated intensity ratio is also shown in **Table 6**. The results show that the average direction to the light sources is successfully estimated if $\theta_1 \leq \frac{1}{6}\pi$, $\theta_2 \leq \frac{1}{6}\pi$ [rad]. On the contrary, in Section 6.3 we showed that it is possible to estimate the light direction accurately if the angle of the light source is $\frac{1}{4}\pi$ [rad] or less, because multiple light sources decrease the area of inliers. However, the experimental results show that the proposed algorithm is able to handle a case with multiple light sources.

Table 4 Error in estimated angle of average light direction in image 1 [rad].

		θ_2 (angle of L_{12} and L_{22}) [rad]				
		0	$\frac{1}{12}\pi$	$\frac{1}{6}\pi$	$\frac{1}{4}\pi$	$\frac{1}{3}\pi$
θ_1 (angle	$\frac{1}{12}\pi$	0.042	0.036	0.013	0.410	0.566
of L_{11}	$\frac{1}{6}\pi$	0.017	0.005	0.000	0.458	0.576
and L_{21})	$\frac{1}{4}\pi$	0.035	0.012	0.406	0.343	0.698
[rad]	$\frac{1}{3}\pi$	0.586	0.139	0.575	0.675	0.519

Table 5 Error in estimated angle of average light direction in image 2 [rad].

		θ_2 (angle of L_{12} and L_{22}) [rad]				
		0	$\frac{1}{12}\pi$	$\frac{1}{6}\pi$	$\frac{1}{4}\pi$	$\frac{1}{3}\pi$
θ_1 (angle	$\frac{1}{12}\pi$	0.035	0.033	0.025	0.229	0.057
of L_{11}	$\frac{1}{6}\pi$	0.030	0.003	0.000	0.131	0.207
and L_{21})	$\frac{1}{4}\pi$	0.019	0.031	0.297	0.454	0.692
[rad]	$\frac{1}{3}\pi$	0.420	0.362	0.433	0.753	1.163

Table 6 Error in the intensity ratio of light sources.

		θ_2 (angle of L_{12} and L_{22}) [rad]				
		0	$\frac{1}{12}\pi$	$\frac{1}{6}\pi$	$\frac{1}{4}\pi$	$\frac{1}{3}\pi$
θ_1 (angle	$\frac{1}{12}\pi$	0.000	0.001	0.006	0.550	0.712
of L_{11}	$\frac{1}{6}\pi$	0.011	0.007	0.000	0.639	0.681
and L_{21})	$\frac{1}{4}\pi$	0.027	0.019	0.162	0.133	0.121
[rad]	$\frac{1}{3}\pi$	0.7377	0.166	0.525	0.128	33.784

7. Experiments with Actual Images

In this section we show the experimental results for captured images of actual objects. The first experiment is carried out indoors with an artificial light source, while the second is conducted outdoors using the movement of sunlight.

7.1 Indoor Experiments

In this section, we show two results using actual images taken by a camera. **Figure 8** shows the two objects used in the experiments and their rendered images with measured shapes. The sphere and its measured shape are common

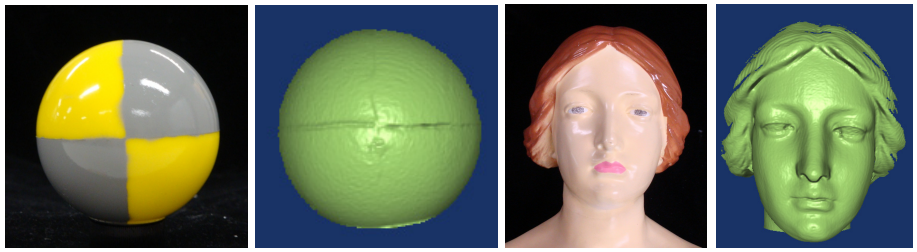

(a) (b) (c) (d)

Fig. 8 Objects used in the experiments: (a) sphere with two reflectances, (b) measured shape of the sphere, (c) statue with specular reflection, (d) measured shape of the statue.

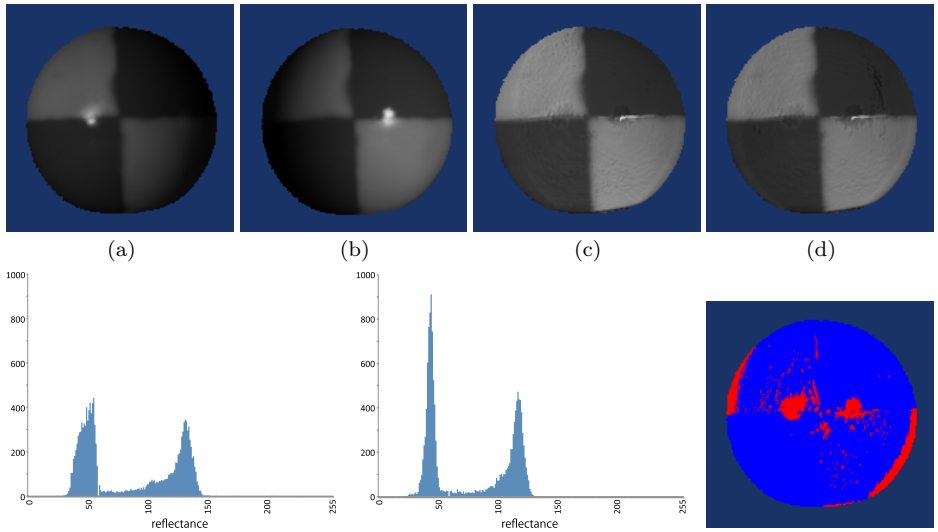

(a) (b) (c) (d) (e) (f) (g)

Fig. 9 Experimental results for the sphere: (a)(b) input images, (c) estimated albedo map using all sample points, (d) estimated albedo map with robust estimation, (e) albedo histogram of (c), (f) albedo histogram of (d), (g) map of outliers found by robust estimation.

to the simulation experiments.

Figures 9 (a) and (b) show the two input images for the experiment. The estimated albedo maps using all sample points and robust estimation are shown in Figs. 9 (c) and (d), respectively. In this case, no obvious difference is seen in the estimated albedo maps because any albedo value estimated at a pixel with specular reflection is excluded by the method described in Section 4.3. However, it is clearly shown that the distribution of estimated albedo in Fig. 9 (f) has two obvious peaks that are higher than the result in Fig. 9 (e). Eigenvalues of the PCA calculation are shown in **Table 7**. The ratio of the 6th to 5th eigenvalues is much improved. Figure 9 (g) shows the distribution of the outliers with the region of specular reflection correctly excluded.

Table 7 Contribution rate of PCA for "sphere" object.

	1st eigenvalue	5th eigenvalue	6th eigenvalue
estimation using all samples	0.485684	0.017551	0.010500
robust estimation	0.536442	0.009747	0.001296

Next we used a colored statue with specular and interreflection at the concave areas. **Figures 10** (a) and (b) show the two input images for the experiment. Estimated albedo maps using all sample points and robust estimation are shown in Figs. 10 (c) and (d), respectively. In this case, it is clear that the albedo map calculated with robust estimation is more uniform than that using all the samples. While the actual directions of the light sources are unknown, we think that the estimation of the light direction is badly affected by specular reflection, interreflection, and shadow.

Eigenvalues of the PCA calculation are shown in **Table 8**. The ratio of the 6th to 5th eigenvalues is much improved. Figure 9 (e) shows the distribution of outliers. In this case, the region of outliers is widely spread because of the shadow, specular reflection and interreflection, but the convex areas without such effects seem to contribute correctly to the estimation. The estimated albedo is affected by the increased intensity of the interreflection, and we see the effect thereof in Fig. 10 (d). To solve the problem, an inverse rendering method, which handles interreflection [18], could also be used with information of the estimated light directions.

7.2 Experiment Using the Movement of Sunlight

One of the main advantages of our method is its ability to estimate albedo using the movement of sunlight. Since the movement of the sun is almost coplanar, most methods based on photometric stereo framework do not work with sunlight. On

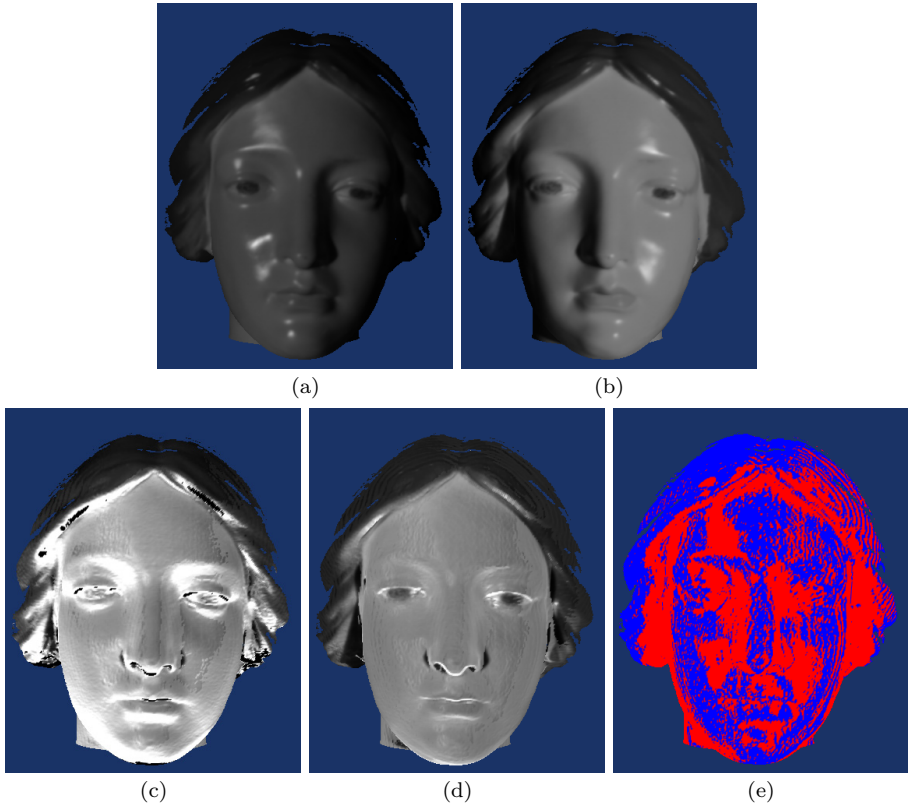

(a) (b) (c) (d) (e)

Fig. 10 Experimental results for the colored statue: (a)(b) input images, (c) estimated albedo map using all sample points, (d) estimated albedo map with robust estimation, (e) map of outliers found by robust estimation.

Table 8 Contribution rate of PCA for "statue" object.

	1st eigenvalue	5th eigenvalue	6th eigenvalue
estimation using all samples	0.464233	0.015473	0.011574
robust estimation	0.522036	0.015878	0.002420

the contrary, our method is applicable in this case because we only use two images. Since it is not easy to evaluate the preciseness of albedo map estimation, we use an object with homogeneous reflectance and check the uniformity of estimated albedo map.

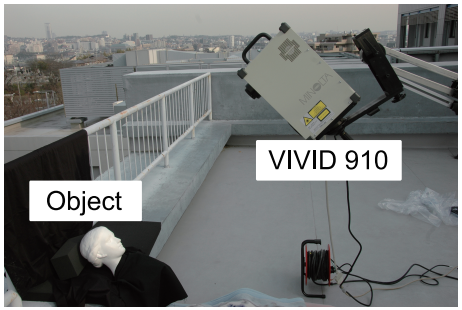

Fig. 11 Experimental setup using the movement of sunlight.

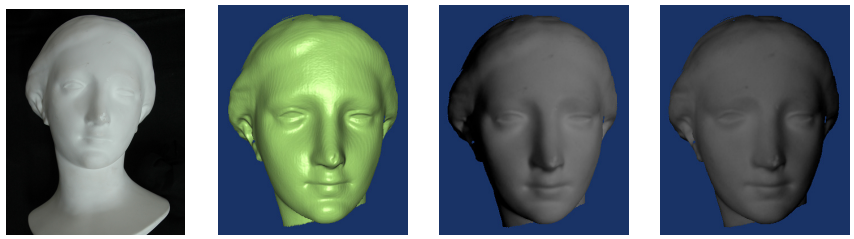

(a) Appearance of the object (b) Shape of the object (c) Image 1, taken at 11:13 (d) Image 2, taken at 14:11

Fig. 12 Object and images for the outdoor experiment.

The shape of the object is measured using a rangefinder (Minolta VIVID 910). Intensity images are also captured by the rangefinder with an ND filter because sunlight is too bright to capture an image without saturation. The experiment was carried out on January 20th, 2010, and the outdoor experimental setup is shown in **Fig. 11**. We confirmed that the day was sunny. We took two intensity images at 11:13am and 2:11pm, and the shape of the object was measured after sunset. The object used in the experiment is shown in **Fig. 12** (a), while the rendered image of the measured shape is shown in Fig. 12 (b). The images shown in Figs. 12 (c) and (d) are the captured images taken at 11:13 and 14:11, respectively.

The experimental results are shown in **Fig. 13**. Figures 13 (a) and (b) show

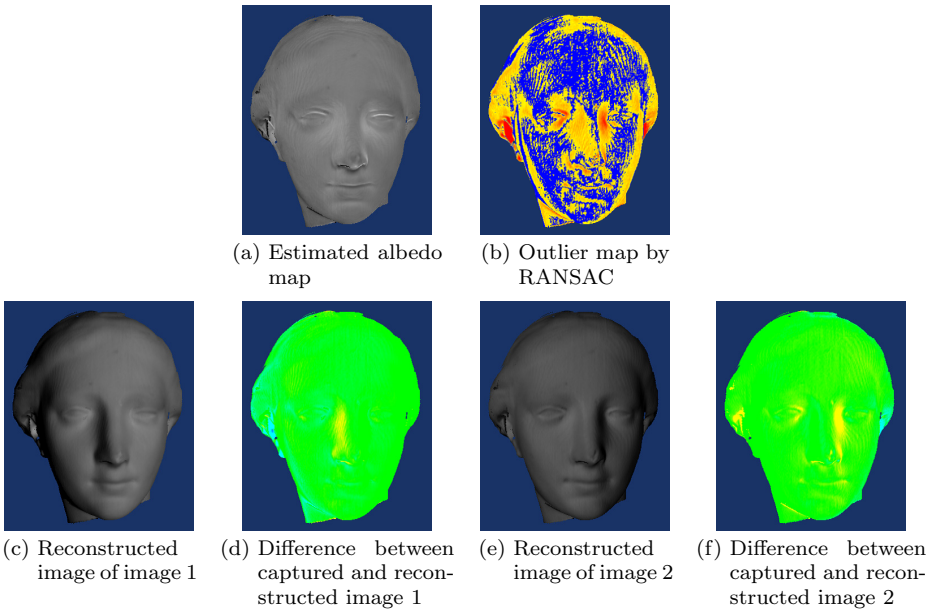

(a) Estimated albedo map (b) Outlier map by RANSAC

(c) Reconstructed image of image 1 (d) Difference between captured and reconstructed image 1 (e) Reconstructed image of image 2 (f) Difference between captured and reconstructed image 2

Fig. 13 Experimental results using the movement of sunlight.

Table 9 Evaluation of the angle between two light sources [rad].

Angle calculated by the time of capture	0.7588
Angle between two estimated light directions	0.7767
Error in angle	0.0179

the albedo and outlier maps estimated by RANSAC. Figure 13 (c) is the rendered image of image 1 using the estimated albedo map and light direction. The difference between the captured and reconstructed image is shown in Fig. 13 (d) where green means that the error is close to zero. Figures 13 (e) and (f) show the rendered image and its error compared to image 2.

The angle between two light sources can be calculated using the interval between the times at which images 1 and 2 were captured, and this can be used as a true value. The angle of the movement of sunlight is 0.7588 [rad], while the estimated one is 0.7767 [rad] (**Table 9**). The difference 0.0179 [rad] (1.02 [deg], corresponding to 4 minutes in time) is sufficiently small.

The greater part of the reconstructed albedo map is homogeneous, which shows a successful estimation. However, it also shows the effect of shadow and interreflection at the concave-shaped parts. The outlier map also shows that parts with a concave shape tend to be classified as outliers. This shows that interreflection is also successfully excluded by the robust estimation with RANSAC.

8. Conclusion

We proposed a method to determine the light direction and diffuse reflectance property of two images under different lighting conditions. By using information about the shape of the object, we derived a relationship between the light direction and diffuse reflectance that enables us to estimate both of them simultaneously from 6 or more points on two images. While specular reflection and shadows affect the estimation as outliers and cause errors, we can avoid these outliers by robust estimation using RANSAC. Experimental results show the clear effect of robust estimation, while objects with nonlinear effects such as specular reflection and shadow can be handled with our method for estimating an albedo map.

References

1) Kajiya, J.T.: The rendering equation, *ACM SIGGRAPH*, Vol.20, No.4, pp.143–150 (1986).
2) Horn, B.K.P.: Obtaining shape from shading information, *Shape from Shading*, Horn, B.K.P. and Brooks, M.J. (Eds.), pp.121–171, MIT Press (1989).
3) Woodham, R.J.: Photometric method for determining surface orientation from multiple images, *Optical Engineering*, Vol.19, No.1, pp.139–144 (1980).
4) Argyriou, V. and Petrou, M.: Photometric Stereo: An overview, *Advances in Imaging and Electron Physics*, Vol.156, pp.1–54 (2009).
5) Debevec, P.: Rendering Synthetic Objects Into Real Scenes: Bridging Traditional and Image-Based Graphics With Global Illumination and High Dynamic Range Photography, *Proc. SIGGRAPH 98*, pp.189–198 (1998).
6) Ikeuchi, K. and Sato, K.: Determining reflectance properties of an object using range and brightness images, *IEEE Trans. PAMI*, Vol.13, No.11, pp.1139–1153 (1991).
7) Romeiro, F. and Zickler, T.: Blind Reflectometry, *Proc. European Conference on Computer Vision*, pp.45–58 (2010).

8) Ramamoorthi, R. and Hanrahan, P.: A Signal Processing Framework for Inverse Rendering, *Proc. SIGGRAPH 2001*, pp.117–128 (2001).
9) Zickler, T., Ramamoorthi, R., Enrique, S. and Belhumeur, P.: Reflectance sharing: Predicting appearance from a sparse set of images of a known shape, *IEEE Trans. PAMI*, Vol.28, No.8, pp.1287–1302 (2006).
10) Sato, Y. and Ikeuchi, K.: Reflectance analysis for 3d computer graphics model generation, *CVGIP Graphical Models and Image Processing*, Vol.58, No.5, pp.437–451 (1996).
11) Hara, K., Nishino, K. and Ikeuchi, K.: Mixture of Spherical Distributions for Single-View Relighting, *IEEE Trans. Pattern Analysis and Machine Intelligence*, Vol.30, No.1, pp.25–35 (2008).
12) Hara, K. and Nishino, K.: Illumination and Spatially Varying Specular Reflectance from a Single View, *Proc. CVPR '09*, pp.619–626 (2009).
13) Ramamoorthi, R. and Hanrahan, P.: On the relationship between radiance and irradiance: Determining the illumination from images of a convex lambertian object, *J. Optical Society of America A*, Vol.18, No.10, pp.2448–2459 (2001).
14) Belhumeur, P.N., Kriegman, D.J. and Yuille, A.L.: The Bas-Relief Ambiguity, *International Journal of Computer Vision*, Vol.35, pp.33–45 (1999).
15) Georghiades, A.S.: Recovering 3-D shape and reflectance from a small number of photographs, *Proc. 14th Eurographics Workshop on Rendering*, pp.230–240 (2003).
16) Barsky, S. and Petrou, M.: The 4-source photometric stereo technique for three-dimensional surfaces in the presence of highlights and shadows, *IEEE Trans. PAMI*, Vol.25, No.10, pp.1239–1252 (2003).
17) Fischler, M.A. and Bolles, R.C.: Random Sample Consensus: A Paradigm for Model Fitting with Applications to Image Analysis and Automated Cartography, *Comm. ACM*, Vol.24, pp.381–395 (1981).
18) Machida, T. and Yokoya, N.: Dense Estimation of Surface Reflectance Properties of Objects with Interreflections, *Proc. Int. Conf. on Pattern Recognition* (*ICPR*), Vol.1, pp.348–351 (2002).
19) Nishino, K., Zhang, Z. and Ikeuchi, K.: Determining reflectance parameters and illumination distribution from a sparse set of images for view-dependent image synthesis, *Proc. IEEE ICCV'01*, pp.599–606 (2001).
20) Llado, X., Oliver, A., Petrou, M., Freixenet, J. and Marti, J.: Simultaneous surface texture classification and illumination tilt angle prediction, *Proc. British Machine Vision Conference*, pp.789–798 (1993).

(Received November 9, 2010)
(Accepted August 11, 2011)
(Released December 28, 2011)

(Communicated by *Sang Wook Lee*)

Takehiro Tachikawa graduated from the Faculty of Engineering Science and Graduate School of Engineering Science at Osaka University in 2008 and 2010, respecitively. Currently he is a member of Nikon Corporation. He was engaged in research on photometric analysis of images. He holds a M.Eng. degree.

Shinsaku Hiura dropped out from the Faculty of Engineering Science at Osaka University to skip the 4th grade in 1993, and immediately entered to the Graduate School of Engineering Science there. He completed his doctoral course at Osaka University in 1997, and became a research associate of Kyoto University. In 1999, he became an assistant professor in the Graduate School of Engineering Science at Osaka University, and associate professor in 2003. From 2008 to 2009, he joined the Media Laboratory at Massachusetts Institute of Technology as a visiting associate professor. In 2010, he moved to Hiroshima City University as a professor and currently there. He is engaged in research on computer vision, 3D image analysis and computational photography. In 2000, he received an outstanding paper award from Symposium on Sensing via Image Information. In 2010, he received IPSJ Yamashita SIG Research Award. He holds a D.Eng. degree.

Kosuke Sato completed his master's course at Osaka University in 1985, and became a research associate in Control Engineering on the Faculty of Engineering Science there. From 1988 to 1990, he was a visiting researcher at the Robotics Institute of Carnegie Mellon University (USA). From 1994 to 1999, he was an assistant professor in the Graduate School of Information Science at Nara Institute of Science and Technology. Currently, he is a professor in the Graduate School of Engineering Science at Osaka University. He is engaged in research on 3D image measurement, CV, and virtual reality. In 1998, he received the Shinohara Memorial Promotion of Science Prize. His publications include 3D Image Measurement. He holds a D.Eng. degree.